

Unprecedented Catalysis of Cs⁺ Single Sites Confined in Y Zeolite Pores for Selective C_{sp3}-H Bond Ammoxidation: Transformation of Inactive Cs⁺ Ions with a Noble Gas Electronic Structure to Active Cs⁺ Single Sites

*Shankha S. Acharyya,^{‡a,b} Shilpi Ghosh,^{‡a,b} Yusuke Yoshida,^a Takuma Kaneko,^a Takehiko Sasaki,^{‡*c} Yasuhiro Iwasawa^{‡*a,b}*

^a Innovation Research Center for Fuel Cells, The University of Electro-Communications, Chofu, Tokyo 182 8585, Japan

E-mail: iwasawa@pc.uec.ac.jp

^b Graduate School of Informatics and Engineering, The University of Electro-Communications, Chofu, Tokyo-182 8585, Japan

^c Graduate School of Frontier Science, The University of Tokyo, Kashiwa, Chiba 277-8561, Japan

E-mail: takehiko@k.u-tokyo.ac.jp

KEYWORDS: Catalytic C_{sp3}-H activation • Confined Cs⁺ single site in Y zeolite pore • Ammoxidation of toluene and its derivatives • Selective nitrile synthesis • Catalysis mechanism

ABSTRACT: We report the transformation of Cs⁺ ions with an inactive noble-gas electronic structure to active Cs⁺ single sites chemically confined in Y zeolite pores (Cs⁺/Y), which provides an unprecedented catalysis for oxidative cyanation (ammoxidation) of C_{sp3}-H bonds with O₂ and NH₃ though in general, alkali and alkaline-earth metal ions without moderate redox property cannot activate C_{sp3}-H bonds. The Cs⁺/Y catalyst was proved to be highly efficient in synthesis of aromatic nitriles with higher yields than 90% in the selective ammoxidation of toluene and its derivatives as test reactions. The mechanisms for the genesis of active Cs⁺ single sites and ammoxidation pathway of C_{sp3}-H bonds were rationalized by DFT simulations. The chemical confinement of large-sized Cs⁺ ions with the pore architecture of Y zeolite supercage rendered the HOMO–LUMO gap reduction, HOMO component change and preferable coordination arrangement for the selective reaction promotion, which provides a trimolecular assembly platform to enable the coordination-promoted concerted ammoxidation pathway working closely on each Cs⁺ single site. The new reaction pathway without involvements of O₂-dissociated O atom and lattice oxygen differs from the traditional redox catalysis mechanisms for the selective ammoxidation.

1. INTRODUCTION

Alkali metal ions with inactive noble gas electronic structures have been conceived as inactive species for selective functionalization of C_{sp2}-H and C_{sp3}-H bonds to useful chemicals in industry. Recently, we found a single alkali metal ion site platform in β zeolite pore that selectively promoted benzene C_{sp2}-H activation toward phenol synthesis.^{1,2} The catalytic performance of alkali metal ion sites incorporated in zeolite pores depended strongly on the kind of zeolites, and ZSM-5, mordenite and Y zeolites were almost inactive as supports. No C_{sp3}-H activation catalysis of alkali metal ions and oxides has been achieved to date, though a variety of effects of alkali metal additives on metal oxide catalysis are known.³ Here, we report the first example of the catalytic selective activation of C_{sp3}-H bonds to produce C-N bonds on Cs⁺ single ion sites in Y zeolite pores (Cs⁺/Y) due to transformation of inactive Cs⁺ ions with a noble gas electronic

structure to active Cs^+ sites with HOMO(O 2p)–LUMO(Cs 6s) by chemical confinement of Cs^+ ions at Y zeolite pore surfaces, making Cs-O bonds and reactive coordination. Ammoxidation of methyl C_{sp^3} -H bonds of aromatics with O_2+NH_3 is an avenue for the synthesis of organic nitriles, which have been commercially used as common building blocks for high-performance rubbers, polymers and molecular electronics, and also as integral parts for producing pharmaceuticals, agrochemicals and fine chemicals, such as vitamins, heterocycles and various carboxylic acid derivatives.^{4,5} Generally, organic nitriles were synthesized by cyanation of aldehydes using toxic hydrogen cyanide and metal cyanides which caused environmental disasters.^{3,6-9} Industrially, the vapor phase ammoxidation of toluene to benzonitrile has been extensively studied with metal and metal oxide catalysts of V, Cr, Mo, etc.,¹⁰⁻²⁵ whose catalysts possess moderate redox potentials and sufficient M–O bond strengths to provide active lattice oxygen and oxygen atoms at the catalyst surfaces for the redox catalysis. The Cs^+/Y catalyst without a beneficial redox property showed a high benzonitrile yield (92.7%; 94.6% conversion and 98.0% selectivity at 623 K) and a high NH_3 utilization efficiency (almost no extra consumption) in toluene ammoxidation employed as test reaction; to the best of our knowledge, this is the highest yield without NH_3 loss for the benzonitrile synthesis from toluene with O_2+NH_3 in a single-step gas-phase reaction. There is always a competition between the ammoxidation to benzonitrile and undesirable NH_3 oxidation to N_2 and NO_x on catalyst surfaces,^{1-3,11,23} whereas the Cs^+/Y was found to catalyze no NH_3+O_2 reaction when toluene was not present (Table 1). The simple ion-exchange method for the chemically confined Cs^+/Y catalyst fabrication in this study is also advantageous in industrial usage. The Cs^+/Y catalyst was also effective in synthesis of other organic nitriles, thereby proving its versatility. The genesis and mechanism of the unprecedented catalysis by the Cs^+ single ion site/Y, which differs from the traditional redox catalysis mechanisms, has been characterized by XPS, STEM-EDS, XRD, TPD, *in situ* XANES and EXAFS, and DFT calculations.

2. EXPERIMENTAL SECTION

Catalyst Synthesis. Zeolite Y-supported alkali metal ion and alkaline-earth metal ion catalysts were prepared by a reliable ion exchange method,^{1,2} followed by a controlled treatment at 573 K,

using the corresponding metal nitrates as precursors. A typical Cs(2 wt%)/Y sample was synthesized as follows. CsNO₃ 0.88 g (Kanto Chemical Co.) was dissolved in 10 ml of deionized water in a 50 ml Erlenmeyer flask, to which 2.91 g of NH₄-Y with SiO₂/Al₂O₃= 30 (purchased from Zeolyst Co.) was added with stirring. For ion-exchange of NH₄⁺ ions with Cs⁺ ions, the solution was heated from room temperature to 353 K and maintained at 353 K for 12 h with stirring, followed by washing with deionized water and centrifuging, and finally drying at 353 K for 8 h. Other zeolite Y-supported alkali and alkaline-earth metal ion catalysts were prepared similarly. Cs⁺(2 wt%)/Y samples with different SiO₂/Al₂O₃ ratios (5.2, 5.6, 12, and 115) were also prepared in the similar way. Furthermore, other supports for Cs⁺ (β, ZSM-5, mordenite (Mor), hydrotalcite (Hydr) and silica-alumina (SiO₂•Al₂O₃) were also used to prepare different supported Cs⁺ catalysts for comparison.

Catalytic Reactions and Product Analysis. Vapor phase ammoxidation of toluene was carried out at atmospheric pressure using a fixed-bed flow reactor (Pyrex glass tube) with an inner diameter of 6 mm and externally heated by electric resistances. The reaction temperature was measured inside the catalyst bed by a thermocouple, whose tip was placed inside the upper side of the catalyst bed. Catalyst powders were pressed to pellets, crushed, and sieved (typically, 0.2 g, sieved into 500-850 μm particles), and the sieved samples were packed between quartz wools in the flow reactor. Toluene was fed continuously into the gas stream by using a syringe pump. The reactor was fed with toluene/NH₃/O₂/He mixture in the molar ratio of 0.20/1.8/1.0/5.0 ml min⁻¹ typically. The flow ratio of NH₃ to toluene was deliberately kept ~ 9 times larger in order to increase the nitrile selectivity since the formation of CO₂ decreases considerably with increasing amounts of NH₃ in the feed. The conversion and selectivity in the current system were calculated by using NH₃ as an internal standard taking into account the calibration factors for NH₃ in the FID and TCD GCs in a similar way to that in our previous reports, assuming no loss of nitrogen in the material balance during the catalytic reactions.¹ The outlet stream was sampled with six-way sampling valves heated at 463 K using an online Shimadzu GC-2014 with a FID using a ZB-WAX plus capillary column (30 m, Phenomenex CA) for NH₃, toluene and benzonitrile, and a Shimadzu GC-2014 with a TCD using a WG-100 column (GL Science Japan) for O₂, N₂, CO, CO₂, NH₃ and H₂O. Helium was used as carrier gas. The column temperature for TCD was 323 K. The column temperature for FID was held at 413 K for the first 2 min and then increased to 473 K at a heating rate of 298 K min⁻¹. For the ammoxidation of toluene in the present system,

the nitrogen containing products were N₂ and benzonitrile (PhCN) with a negligible amount of PhCONH₂. GC-TCD analysis showed no formation of N₂O. The elemental carbon and nitrogen mass balances were estimated to be the values between 97% and 100% in most of the experimental runs.

Temperature Programmed Desorption (TPD). All TPD experiments were carried out in a flow reaction system in a flow of helium carrier gas (50 ml min⁻¹). For each experiment in a fixed-bed reactor (6 mm i.d.) 0.2 g catalysts with similar grain sizes (0.2–0.4 mm) were used. The catalysts were heated under He flow (4 ml min⁻¹) at 573 K for 30 min and cooled down to adsorption temperature (300 K). Respective flows of CO₂ and CH₃CN were turned on 5 ml min⁻¹ and kept for 15 min to complete their adsorption. The samples after the adsorption were flushed with helium (40 ml min⁻¹) for 15 min, then heated in a ramping rate of 28.3 K min⁻¹. The analysis of reactor effluents (CO₂ and CH₃CN) was performed on gas chromatographs with a thermal conductivity detector (TCD) and a flame ionization detector (FID), respectively, calibrated by the peak area of known pulses of the respective chemicals. NH₃ TPD experiments on Cs⁺(2 wt%)/Y and Cs⁺(2 wt%)/β at 353–923 K were also conducted in a similar way to the above TPD experiments to examine the adsorption behavior and strength of NH₃ in relation to ammoxidation catalysis mechanism.

***In Situ* XAFS Measurements and XAFS Data Analysis.** *In situ* XAFS spectra at Cs L₃-edge for the as-synthesized Cs⁺(2 wt%)/Y sample and after the pre-treatment and catalysis of the sample without exposing air were measured at 15 K in a fluorescence mode at BL36XU station in SPring-8. XANES and EXAFS spectra were analyzed in the similar way to the previous reports,^{1,26} using the Larch code containing the IFEFFIT Package ver.2 (Athena and Artemis).²⁷ Background subtraction in the EXAFS analysis was performed using Autobk.²⁸ The Victoreen function was employed for the background subtraction and the spline smoothing method with Cook and Sayers criteria was used as the μ₀ method. The extracted k²-weighted EXAFS oscillations were Fourier-transformed to R-space over k = 25–80 nm⁻¹, and the curve fittings were performed in the R-space (0.18–0.32 nm). The fitting parameters for each shell were coordination number (CN), interatomic distance (R), Debye-Waller factor (σ²), and correction-of-edge energy (ΔE₀). The phase shifts and amplitude functions for Cs–O and Cs–Cs were

calculated from the FEFF 8.4 code.²⁹ Error ranges of the curve-fitting analysis of EXAFS Fourier transforms were based on the definition of the Larch code.²⁷

DFT Calculations. All calculations were conducted with Dmol3 ver. 2018 (Biovia) on Materials Studio 2018.^{30,31} Numerical basis set with polarization function (DNP), of which quality is comparable to 6-31G*, was adopted. All electrons were explicitly included. All possible multiplicities of electronic states were compared in the calculations and optimized multiplicity was determined in each system. Perdew-Wang 91 functional (PW91)³² was used in all the calculations. Transition states were searched by Dmol3 with the complete QST/LST option, where the Linear Synchronous Transit (LST) maximization was performed for the coordinates interpolated between a reactant and a product, followed by repeated conjugated gradient minimizations and the Quadratic Synchronous Transit (QST) maximizations until a transition state has been located.^{33,34}

To include the HY (Faujasite: FAU) zeolite framework, a cluster containing 6-membered ring with neighboring twelve 4-membered rings was taken from the crystal structure of FAU zeolite with hydrogen atom-termination (Si-H). One Si atom in the 6-membered ring was replaced by Al atom with adding H atom on the neighboring oxygen atom. Positions of Al atom, the added H atom and neighboring oxygen atoms were relaxed in the structural optimization. Then the H atom was replaced by Cs atom and the positions of Cs atom, Al atom and neighboring O atoms were relaxed. The model (Cs₁Si₂₃Al₁O₃₇H₂₃) obtained in this way was used to examine the adsorption of toluene, O₂ and NH₃ and subsequent intermediates and transition states. Plots for density of states were drawn with respect to the Fermi level corresponding to the midpoint between HOMO and LUMO as the origin.

3. RESULTS AND DISCUSSION

3.1. Catalytic performances of Cs⁺/Y and other supported alkali and alkaline-earth metal ions. We have examined catalytic performances of alkali and alkaline-earth metal ions, which were chemically confined in various zeolite pores and hydrotalcite interlayers, and supported on SiO₂•Al₂O₃ surface, in gas phase ammoxidation (oxidative cyanation) of toluene with O₂ and NH₃ on 0.2 g catalysts at 623 K as a test reaction. The results are shown in Table 1.

Alkaline-earth metal ions (Mg^{2+} , Ca^{2+} , Sr^{2+} , Ba^{2+})/Y samples (Y zeolite: $\text{SiO}_2/\text{Al}_2\text{O}_3$ molar ratio=30) were incapable of activating $\text{C}_{\text{sp}^3}\text{-H}$ bonds as expected, and alkali metal ions (Na^+ and K^+)/Y samples also showed insufficient activity for benzonitrile (PhCN) synthesis, whereas Rb^+ /Y and particularly Cs^+ /Y possessed great potential to functionalize toluene $\text{C}_{\text{sp}^3}\text{-H}$ bond toward PhCN; the toluene conversion was 47.1% and 73.0%, respectively, and the PhCN selectivity was high as 98.1% and 98.5%, respectively, and only a by-product was CO_2 and no other liquid by-products were observed. It is noteworthy that the Rb^+ /Y and Cs^+ /Y catalysis

Table 1. Catalytic performances of various alkali and alkaline-earth metal ion single sites in different zeolite pores and hydrotalcite interlayers and on $\text{SiO}_2\cdot\text{Al}_2\text{O}_3$ surface for the toluene ammoxidation to benzonitrile (PhCN) at 623 K ^[a]

Entry	Catalyst	Toluene Conv./%	PhCN Selec./%	PhCN Syn. Rate/ $\mu\text{mol s}^{-1} \text{g}^{-1}_{\text{cat}}$	NH_3/PhCN
1	Y zeolite	0	–	0	–
2	Mg^{2+} (2 wt%)/Y	2.2	97.8	0.017	18.1
3	Ca^{2+} (2 wt%)/Y	5.1	97.5	0.04	19.4
4	Sr^{2+} (2 wt%)/Y	9.0	97.0	0.08	10.0
5	Ba^{2+} (2 wt%)/Y	11.2	97.5	0.09	14.6
6	Na^+ (2 wt%)/Y	4.9	98.9	0.04	2.8
7	K^+ (2 wt%)/Y	17.6	98.5	0.14	2.1
8	Rb^+ (2 wt%)/Y	47.1	98.1	0.40	1.2
9	Cs^+ (2 wt%)/Y	77.1	98.5	0.60	1.0
10	Cs^+ (2 wt%)/ β	31.3	97.3	0.23	2.1
11	Cs^+ (2 wt%)/ZSM-5	1.0	79.3	0.006	173
12	Cs^+ (2 wt%)/Mor	1.0	86.1	0.006	411
13	Cs^+ (2 wt%)/Hydr	0.2	0	0	–
14	Cs^+ (2 wt%)/ SiAlO_x	0.03	0	0	–
15	Cs^+ (2wt%)/Y ^[b]	34.8	98.9	0.27	2.0
16	Cs^+ (2wt%)/Y ^[c]	93.7	96.6	0.71	5.0
17	Cs^+ (2wt%)/Y ^[d]	94.6	98.0	0.36	1.3
18	Cs^+ (2wt%)/Y ^[e]	0	–	0	–
19	Cs^+ (2wt%)/Y ^[f]	0	–	0	–
20	Cs^+ (2wt%)/Y ^[g]	0 ^[h]	–	–	–

Y: Y zeolite with $\text{SiO}_2/\text{Al}_2\text{O}_3$ molar ratio of 30, purchased from Zeolyst Co. Conv.= conversion. Selec.= selectivity. NH_3/PhCN : molar ratios of consumed NH_3 to synthesized PhCN. Zeolites: Y, β , ZSM-5, and Mordenite (Mor). Hydr: hydrotalcite. SiAlO_x : $\text{SiO}_2\cdot\text{Al}_2\text{O}_3$ with the same $\text{SiO}_2/\text{Al}_2\text{O}_3$ molar ratio (30) as Y zeolite. Performance values: averaged during 30–240 min time-on-stream. Reaction conditions: [a] toluene/ $\text{O}_2/\text{NH}_3/\text{He}$ = 0.20/1.0/1.8/5.0 (ml min^{-1}); cat.= 0.2 g. [b] 603 K. [c] 673 K. [d] 0.4g, 623 K. [e] toluene+ O_2 ; toluene/ O_2/He = 0.20/1.0/5.0 (ml min^{-1}). [f] toluene+ NH_3 ; toluene/ NH_3/He = 0.20/1.8/5.0 (ml min^{-1}). [g] O_2+NH_3 ; $\text{O}_2/\text{NH}_3/\text{He}$ = 1.0/1.8/5.0 (ml min^{-1}). [h] NH_3 conversion/%.

showed a remarkable suppression of undesirable NH_3 oxidation to N_2 and NO_x ; the ratios of $\text{NH}_3(\text{consumed})/\text{PhCN}(\text{synthesized})$ were 1.2 and 1.0, respectively, which are nearly stoichiometric in the ammoxidation reaction equation, $\text{C}_6\text{H}_5\text{CH}_3 + 3/2 \text{O}_2 + \text{NH}_3 \rightarrow \text{C}_6\text{H}_5\text{CN}(\text{PhCN}) + 3 \text{H}_2\text{O}$.

To examine the influence of zeolite compositions ($\text{SiO}_2/\text{Al}_2\text{O}_3$ molar ratios) on the Cs^+/Y catalysis, the toluene ammoxidation on $\text{Cs}^+(2 \text{ wt}\%)/\text{Y}$ samples with different Si/Al ratios was performed. The results are shown in Table S1 (Supporting Information). It was observed that the $\text{Cs}^+(2 \text{ wt}\%)/\text{Y}$ with $\text{SiO}_2/\text{Al}_2\text{O}_3=12$ showed a similar selectivity of 94.8% to 98.0% for the $\text{Cs}^+(2 \text{ wt}\%)/\text{Y}$ with $\text{SiO}_2/\text{Al}_2\text{O}_3=30$, while keeping a high toluene conversion (98.5%), but undesired extra NH_3 oxidation to N_2 became about double under the reaction conditions in Table S1. By more decreasing the $\text{SiO}_2/\text{Al}_2\text{O}_3$ ratio to 5.2–5.6, the selectivity toward benzonitrile decreased to 80.0–81.3% at 97.2–93.1% conv., which indicates that strong Brønsted acidic sites in Y zeolite promote the formation of undesired products (mainly CO_2) and the undesired NH_3 oxidation. When the $\text{SiO}_2/\text{Al}_2\text{O}_3$ ratio was high as 115, the toluene conversion abruptly decreased to 14.2% (Table S1), indicating the necessity of proton sites enough for ion exchange with Cs^+ ions favorably near surface layers of zeolite particles. $\text{Cs}^+(2 \text{ wt}\%)/\text{Y}$ with $\text{SiO}_2/\text{Al}_2\text{O}_3$ molar ratio=30 among the samples examined in this study was proved to be the most superior one.

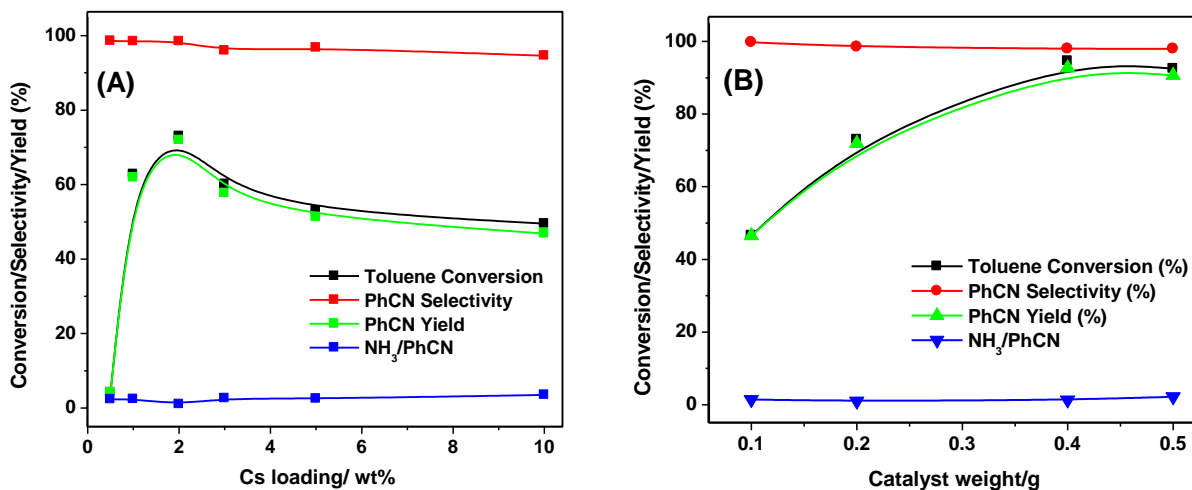
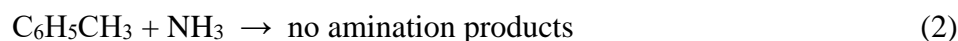


Figure 1. Catalytic activity of Cs^+/Y vs Cs loading (0.2 g-cat) (A) and catalyst weight (B).

The performance (PhCN yield) of Cs⁺/β was 40% of that of Cs⁺/Y as shown in Table 1. Other zeolites such as ZSM-5 and Mordenite (Mor) were not effective as support for Cs⁺ (0.79% and 0.86% yields, respectively; Table 1). Cs⁺/Hydrotalcite (Hydr), where Cs⁺ ions are located in the interlayers of hydrotalcite, showed no activity for the ammoxidation. Cs⁺/SiO₂•Al₂O₃ with the same SiO₂/Al₂O₃ molar ratio (30) as Y zeolite, where Cs⁺ ions were supported on the SiO₂•Al₂O₃ surface was inactive (Table 1). These results suggest importance of the pore architecture of Y zeolite to confine Cs⁺ chemically at the pore surface, thereby inactive Cs⁺ ions with a noble gas electronic structure were transformed to active Cs⁺ ion sites. Effect of Cs loading in 0.2 g Cs⁺/Y on the catalytic performance at 623 K was examined in the Cs loading range of 0.5–10.0 wt% as shown in Figure 1 and Table S2. The activity of the Cs⁺ ions varied with the amount of Cs⁺ ions in Y zeolite. The conversion and selectivity gradually decreased to a saturated level after a maximum at 2.0 wt% Cs loadings. The decrement of the catalytic activity of Cs⁺/Y catalysts with increasing Cs loadings above 2.0 wt% may be attributed to decreasing accessibility of Cs⁺ sites at deeper layers of zeolite particles. At the moment we cannot discuss in more detail on the influence of Cs loadings on the structure of confined Cs⁺ sites and the kinetic regime of ammoxidation over different Cs⁺/zeolites under reaction conditions used in this study. Instead, we have provided Figure S1 and Figure S2 (Supporting Information) displaying the influence of Cs loadings (1, 2, 3, 5, and 10 wt%) on the steady state time-on-stream for the toluene ammoxidation, where all the Cs⁺/Y catalysts showed stable performances under the present conditions. The Cs⁺/Y catalyst with 2.0 wt% Cs loading was the most superior one. The conversion and yield increased with an increase of the catalyst weight up to 0.4 g (for example, the conversion increased from 73.0% to 94.6% with a catalyst increase from 0.2 g to 0.4 g, while keeping a high selectivity of 98.0% (Table 1, Table S3 and Figure 1)) and then the value was saturated, where most of fed toluene molecules were transformed to benzonitrile (94.6% conversion), thereby bringing about nearly no supply to the remaining catalyst layer located close to the reactor exit (eg. 0.1 g in 0.5 g catalyst) (Figure 1 and Table S3). When the catalyst increased above 0.4 g, the undesirable extra NH₃ oxidation (consumed NH₃/synthesized PhCN) increased (Table S3).

Neither bi-components reactions of toluene+O₂ (without NH₃) (eq.1), toluene+NH₃ (without O₂) (eq.2), nor NH₃+O₂ (without toluene) (eq.3) on the Cs⁺/Y proceeded as shown in Table 1 as follows.



The toluene ammoxidation (benzonitrile synthesis) proceeded only in the tri-components reaction (toluene+O₂+NH₃) (eq.4), indicating the contribution of NH₃ to activation of both toluene C_{sp3}-H and O₂ and no contribution of lattice oxygen atoms of the catalyst to the ammoxidation. Thus, the Cs⁺/Y catalyst possesses the unique property; toluene oxidation can be promoted only under the NH₃ coexistence, no toluene amination proceeds, and undesirable NH₃ oxidation with O₂ is suppressed. The activation of both toluene C_{sp3}-H and O₂ by coadsorbed NH₃ and whole ammoxidation pathway on the Cs⁺/Y will be discussed by DFT in 3.3. section. The catalytic performance of Cs⁺(2 wt%)/Y did not change during 240 min time-on-stream (Figure S2), and the pore volume (0.990 cm³ g⁻¹) of the Cs⁺(2 wt%)/Y remained unchanged after 240 min reaction. After 300 min the catalytic conversion at 623 K began to decrease gradually probably due to coking.³⁵ However, the pore volume did not reduce significantly. The performance recovered almost by treatment of the 300 min-spent catalyst at 673 K in air.

Figure 2 shows the plots of the toluene single-path conversion (%) and benzonitrile selectivity (%) on 0.2 g of the alkali (red mark) and alkaline-earth (blue mark) metal ions (2 wt%)/Y catalysts against the ionic radii of alkali and alkaline-earth metal ions to reveal a factor to generate the catalytic performance. In Figure 2 the conversion values for Cs⁺/β, Cs⁺/Mor, Cs⁺/Hydr and Cs⁺/SiO₂•Al₂O₃ are also plotted for comparison. The conversion increased with an increase of alkali and alkaline-earth metal ion radii up to ~0.14 nm, but the performances of their alkali and alkaline-earth metal ions/Y samples were so low as 2.2–17.6% conversions. The Rb⁺/Y and Cs⁺/Y samples with ion radii larger than ~0.14 nm, particularly Cs⁺/Y (Cs⁺ ion diameter: 0.334 nm), showed remarkable conversions with high selectivities (98.1–98.5%). The single Cs⁺ sites cannot activate toluene, O₂, and NH₃ when they get adsorbed independently and also in the case of their bi-components such as toluene+O₂, Toluene+NH₃, and NH₃+O₂ (Table 1). However, when the three-reactants (toluene, O₂, and NH₃) co-adsorbed together, the tri-molecular concerted reaction working closely on the Cs⁺ single metal ion site proceeded efficiently, causing toluene C_{sp3}-H activation toward benzonitrile synthesis.

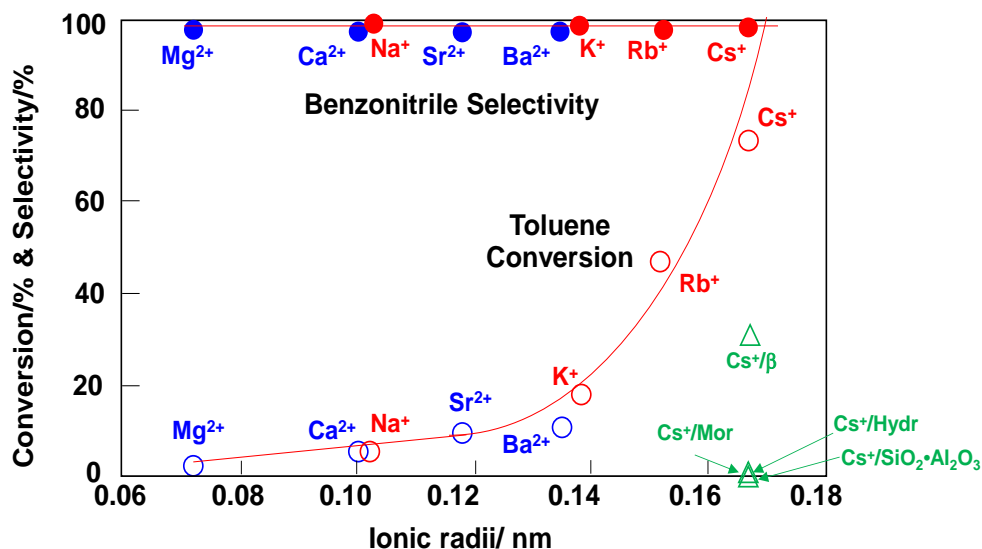


Figure 2. Relation between the catalytic performances (toluene one-path conversion and benzonitrile selectivity) on 0.2 g of the alkali (red mark) and alkaline-earth (blue mark) metal ions (2 wt%)/Y catalysts and the ionic radii of alkali and alkaline-earth metal ions. The conversion values for Cs⁺/β, Cs⁺/mordenite (Mor), Cs⁺/hydrotalcite (Hydr) and Cs⁺/SiO₂·Al₂O₃ are also plotted for comparison. Reaction conditions: see Table 1.

To gain further insight into the nature of accessible sites in the Cs⁺/Y catalyst, the ammoxidation of toluene derivatives with increasing bulkiness was compared with the toluene ammoxidation (Table 2). The Cs⁺/Y catalyst showed good performances in achieving the ammoxidation of *o*-, *m*- and *p*-xylene (81.5–88.8% conv.; 98.0–99.0% selec.), mesitylene (76.2% conv.; 99.8% selec.), and *o*-, *m*- and *p*-chlorotoluene (77.6–91.6% conv.; 94.3–94.6% selec.). With two bulky alkyl benzene molecules, 1,3,5-tri-*t*-butylbenzene and 1,3,5-tris(2,4,6-trimethylphenyl) benzene, no reactions occurred due to the bulkier sizes than the accessible aperture (0.74 nm) of Y zeolite with 3-dimensional network of the open aperture and supercage (1.2 nm),³⁶ in which Cs⁺ ions are confined and bound chemically to pore surface lattice oxygen atoms (as discussed hereinafter).

Table 2. Catalytic performances of Cs⁺(2 wt%)/Y for selective ammoxidation of substituted toluenes at 623 K ^[a]

Entry	Reactant	Reactant Conv./%	Nitrile Selec./%	Nitrile Syn. Rate/ $\mu\text{mol s}^{-1} \text{g}^{-1}_{\text{cat}}$	NH ₃ /Nitrile
1	<i>o</i> -xylene	85.4	98.5 ^[b] (86.6)	0.294	1.0
2	<i>m</i> -xylene	81.5	98.0 ^[b] (78.8)	0.275	1.1
3	<i>p</i> -xylene	88.8	99.0 ^[b] (92.8)	0.300	0.91
4	Mesitylene	76.2	99.8 ^[b] (52.5)	0.228	1.1
5	<i>o</i> -chlorotoluene	81.7	94.5	0.288	0.93
6	<i>m</i> -chlorotoluene	77.6	94.3	0.274	0.98
7	<i>p</i> -chlorotoluene	91.6	94.6	0.322	0.83
8	<i>o</i> -nitrotoluene	42.0	96.0	0.148	1.8
9	<i>m</i> -nitrotoluene	38.0	98.0	0.134	1.9
10	<i>p</i> -nitrotoluene	3.5	99.0	0.012	2.2
11	1,3,5-Tri-tert-butylbenzene	0	–	0	–
12	1,3,5-Tris(2-methylphenyl) benzene	0	–	0	–

Conv.= conversion. Selec.= selectivity. NH₃/Nitrile: molar ratios of consumed NH₃ to synthesized nitriles. Performance values: averaged during 30–240 min time-on-stream. [a] Reaction Conditions: toluene/O₂/NH₃/He= 0.20/1.0/1.8/4.0 (ml min⁻¹); catal.= 0.4 g; reaction temp.= 623 K. [b] Sum of the selectivity (%) of the corresponding mono-nitrile and di-nitrile produced in each entry. The values in the parentheses are the selectivity (%) of the corresponding mono-nitriles.

3.2. Characterization of Cs⁺(2 wt%)/Y by XRD, STEM-EDS and XAFS. To get an insight into the superiority of Cs⁺(2 wt%)/Y we integrated *in situ* and *ex situ* characterization of the Cs⁺(2 wt%)/Y catalysts by XRD (Figure S3), STEM-EDS (Figure S4), XPS (Figure 3 (A)), *in situ* XANES (Figure 3 (B)), *in situ* EXAFS (Figure 3 (C)), DFT simulations (Figure 4, Figure S5 and Figure S6), and TPD (Figure S7). XRD patterns for the Cs⁺/Y samples with 2, 3, 5, 10 wt% Cs loadings exhibited only typical XRD peaks associated with Y zeolite and no Cs oxide peaks were observed up to 10 wt% Cs loadings (Figure S3). Bright-field STEM images and elements (Si, O and Cs) EDS maps for Cs⁺(2 wt%)/Y revealed no feature except for the Y zeolite

lattice (Figure S4). Hence, we measured *in situ* EXAFS data to obtain information on a local coordination structure around Cs site. The observed EXAFS data for Cs⁺(2.0 wt%)/Y

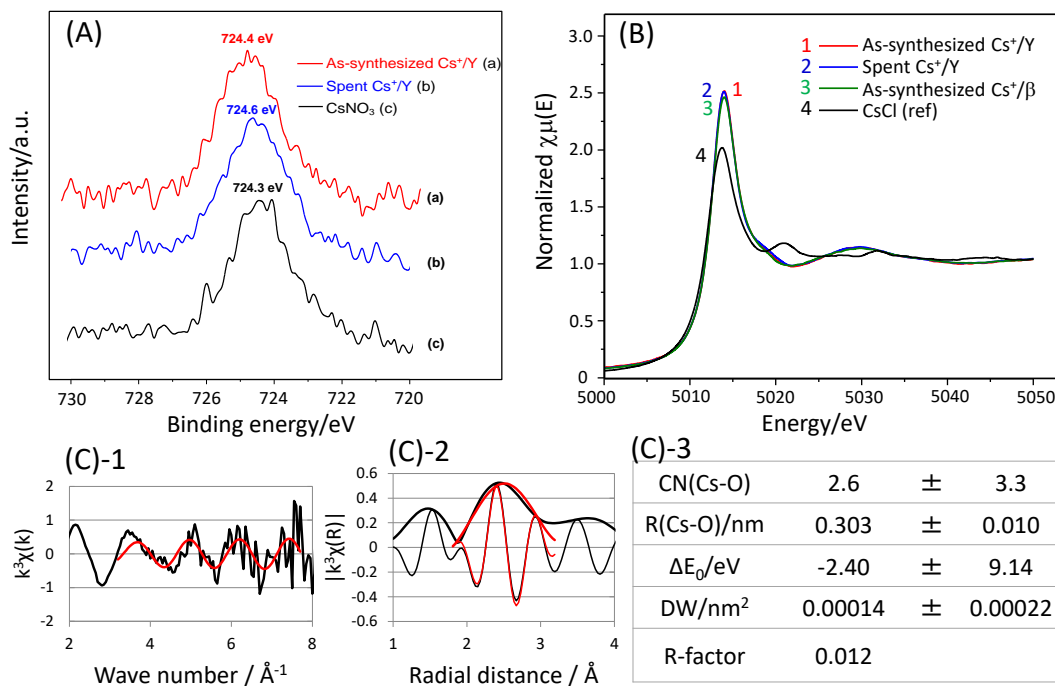


Figure 3. (A) *Ex situ* XPS Cs 3d_{5/2} peaks and binding energies for as-synthesized (fresh) Cs⁺(2 wt%)/Y (a; red), spent Cs⁺(2 wt%)/Y (b; blue) and CsNO₃ (commercial Cs⁺ ion salt) (c; black). (B) *In situ* Cs L₃-edge XANES spectra for as-synthesized (fresh) Cs⁺(2 wt%)/Y (1; red), spent Cs⁺(2 wt%)/Y (2; blue) and Cs⁺(2 wt%)/ β (3; green), and *ex situ* XANES spectrum for CsCl as reference (4; black). (C) *In situ* Cs L₃-edge EXAFS data and analysis for as-synthesized (fresh) Cs⁺(2 wt%)/Y; (C)-1: EXAFS oscillation (black: obs.; red: fitting); (C)-2: EXAFS Fourier transform associated with (C)-1 (black: obs.; red: fitting; gray: imaginary part; orange: fitting); (C)-3: structural parameters for the pretreated Cs/ β determined by EXAFS curve-fitting analysis. The EXAFS data were noisy, but the fitting analysis convincing enough for structural argument was done.

(Figure 3 (C)-1 and (C)-2) were noisy, but we could do the convincing fitting analysis of the EXAFS data enough for structural argument of single Cs⁺ sites. The EXAFS analysis at Cs L₃-edge for the Cs⁺(2 wt%)/Y catalyst in Figure 3 (C) revealed only Cs–O bonds at 0.303 (\pm 0.010) nm with an approximate coordination number of 2.6 and no Cs–Cs bonds were observed, which indicates isolated Cs single sites that are chemically bound to three lattice O atoms of the zeolite pore surface. The experimental results were essentially consistent with the theoretically

simulated structure around Cs⁺ ion in the pore (Cs-O= 0.315, 0.316 and 0.366 nm) in Figure S5, considering that the local structure determined by EXAFS is an averaged coordination structure at every Cs site involved in the catalyst. The coordination structure of Cs sites in Y zeolite pores (Y zeolite component: SiO₂/Al₂O₃=30) resembles that of Cs⁺ single sites in β zeolite pores (β zeolite component: SiO₂/Al₂O₃=30), while the Cs-O interatomic distances are shorter than 0.335, 0.356 and 0.386 nm for Cs⁺/β.¹ The Mulliken charges on Cs⁺ in Y and β pores were estimated as +0.773 and +0.327, respectively by DFT, which is due to the shorter and stronger Cs-O bonds in the Cs⁺/Y than in the Cs⁺/β. It is suggested that the difference in the local structures, Mulliken charges and pore sizes caused the more activity of Cs⁺/Y than Cs⁺/β in the catalytic ammoxidation (Table 1). As to the very poor activity of Cs⁺/ZSM-5 and Cs⁺/MOR, proper local structures around Cs⁺ sites may be obtained for the systems without adsorbed molecules before the ammoxidation catalysis, but rather the narrower pores and channel structures (pore diameter of 0.54 x 0.56 nm for ZSM-5 and one-dimensional pore of 0.67 x 0.70 nm in diameter for Mordenite), compared to pore diameters of 0.55 x 0.55 nm and 0.76 x 0.64 nm for β and a supercage diameter of 1.2 nm and an open aperture of 0.74 nm for Y, may exert steric constraints for a trimolecular concerted pathway involving large sized reaction intermediates and transition states (discussed later), resulting in almost no progress of the ammoxidation reaction on Cs⁺/ZSM-5 and Cs⁺/Mor (Table 1).

Reversely, the Cs⁺/β was active for benzene C_{sp2}-H functionalization toward phenol, but the Cs⁺/Y was inactive for the phenol synthesis.¹ It is to be noted that the activation of C-H bonds by alkali metal ion single sites is very sensitive to the local structure around alkali metal ion. Further, the valency of Cs was proved by XPS 3d spectra and *in situ* XANES (Figure 3 (A) and (B)). The XPS 3d_{5/2} binding energies for the fresh and spent Cs⁺/Y catalysts were 724.7 and 724.6 eV, respectively, which are situated in the values for Cs⁺ mono-cations; 724.3 eV for CsNO₃, 724.5 eV for CsOH, and 724.8 eV for Cs₂CO₃ on Ag. The white line peak intensity in *in situ* Cs L₃-edge XANES spectra for the fresh and spent Cs⁺/Y catalysts was much larger than the *ex situ* XANES spectrum for CsCl with a formal valency of Cs⁺. The white line peak intensity in the XANES spectra at Cs L₃-edge reflects the multielectron photoexcitation feature involving electrons from outer subshells 6s to 4p and it is also related to Cs valency, which resembles the large white line intensity for Cs⁺/β with direct Cs-O bonds.¹ Cs⁺ ions with a noble gas electronic structure coulombically supported on SiO₂ and SiO₂•Al₂O₃ surfaces were inactive for the toluene

ammoxidation (Table 1). Inactive Cs^+ ions were transformed to remarkable Cs^+ single sites confined in Y zeolite pores making direct Cs-O bonds with the Y pore surface lattice oxygen atoms (Table 1, Figure 3 (C) and Figure S5). The density of states (HOMO and LUMO) for Cs^+/Y by DFT calculations using the optimized structural model of Cs^+ single site/Y (Figure S5) is shown in Figure 4 and Figure S6. HOMO and LUMO for free Cs^+ ion is composed of Cs 5p and 6s states, respectively. For the Cs^+ single site chemically confined in Y zeolite making Cs-O bonds, HOMO and LUMO are composed of O 2p state bonding with Al atom at Y pore surface and Cs 6s state on Cs^+ , respectively, as shown in Figure 4, where the HOMO-LUMO gap decreased to 4.7115 eV drastically by increasing HOMO energy and decreasing LUMO energy (Figure 4 and Figure S6). LUMO for Cs^+/β with much less activity than Cs^+/Y constitutes O 2p around Si atom at β pore surface and the HOMO-LUMO gap (5.1059 eV) was larger than that for the Cs^+/Y (Figure S6). The energy gap and nature of HOMO and LUMO states are expected to affect the catalytic performance of the Cs^+ single sites for $\text{C}_{\text{sp}^3}\text{-H}$ bond activation. The above discussion would not be limited to the alkali metal ion single sites in Y zeolite pores. For

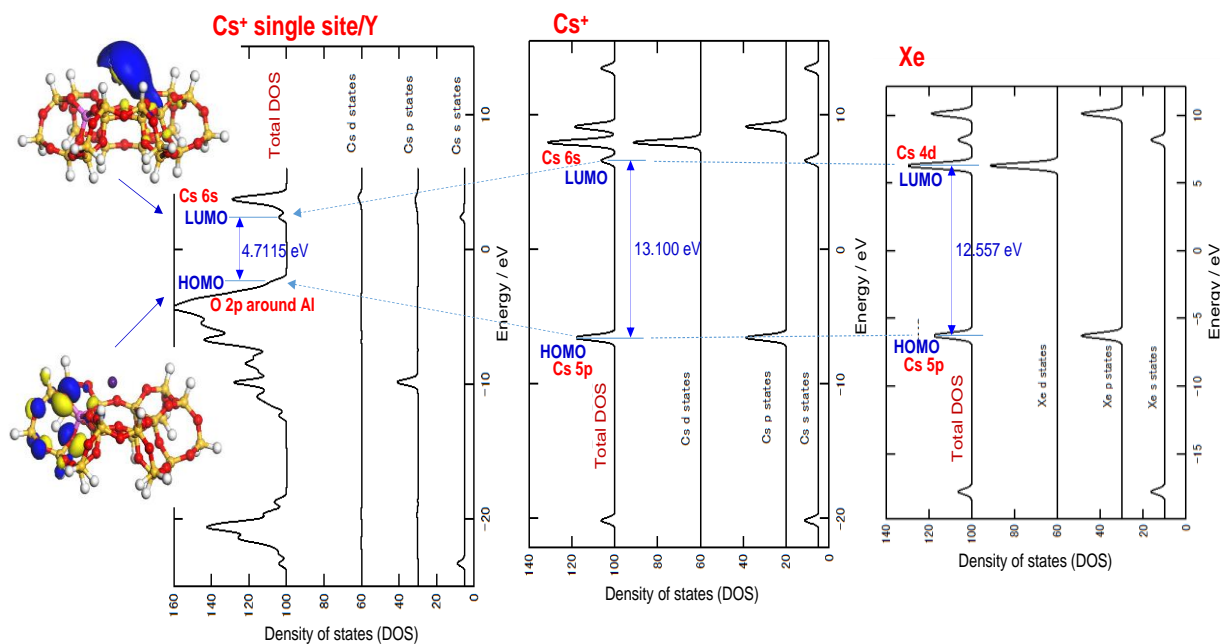


Figure 4. Changes of the energy levels of HOMO and LUMO and the HOMO-LUMO gap by chemical confinement of Cs^+ in Y zeolite pore making Cs-O bonds with pore surface lattice oxygen atoms. Ball-stick model figures for the HOMO and LUMO of Cs^+ single site/Y are also shown.

example, Rh/ZSM-5, in which Rh single atoms were attached on ZSM-5 pore surfaces, has been reported to show unique efficient CH₄ activation toward HCOOH and CH₃COOH at 50 bar though the origin of the unique catalysis of Rh single atom sites/ZSM-5 has not been investigated in detail.³⁷

3.3. Coordination-promoted concerted ammoxidation pathway. Alkali metal ions do not have the moderate redox property that brings about selective oxidation and ammoxidation, which is suggested by the unchanged XPS and XANES spectra in Figure 3. To estimate basic and acidic strengths of the Cs⁺ single sites/Y catalyst, we conducted temperature programmed desorption (TPD) of CH₃CN and CO₂ on Cs⁺(2 wt%)/Y (Figure S7). The TPD peak for CH₃CN on the Cs⁺/Y catalyst was observed at a low temperature around 440 K, and the desorbed CH₃CN amount per Cs⁺ after subtracting the amount desorbed from bare Y zeolite was 66.4% of the Cs⁺ quantity. These results indicate a weak Lewis acidity of the Cs⁺ single sites in Y zeolite pores, which is a little stronger than the Lewis acidity of the Cs⁺ sites in β pores (TPD peak around 360 K). In the TPD of CO₂ on Cs⁺(2 wt%)/Y to estimate the basic strength, most of the adsorbed CO₂ desorbed below 323 K and the desorbed amount was negligible (0.1% of Cs⁺), indicating a negligible basicity of the Cs⁺ single sites in Y pores. Thus, no significant acidity–basicity contribution to the toluene C_{sp3}-H ammoxidation catalysis of Cs⁺(2 wt%)/Y is needed to conceive in the current study.

Although it is generally agreed that activation of the methyl group is the rate determining step during the toluene ammoxidation,^{3,38,39} the nature of activated species and intermediates is still under debate. We examined the effect of electron donating and withdrawing side-groups on the aromatic ring (Table 2). The nitrile yields in the ammoxidation of xylene and chlorotoluene varied in the order: *p*- > *o*- > *m*-substituents unlike that reported previously,⁴⁰ which might be referred to a heterolytic C-H rupture mechanism forming a carbocationic intermediate⁴¹ and involving electronic effects.⁴² In the case of nitrotoluene *p*-nitrotoluene was not converted significantly to *p*-nitrobenzotrile, whereas *o*-nitrotoluene was transformed to the corresponding nitrile with a similar yield to that for *m*-nitrotoluene (Table 2). Further, the carbocationic intermediate should be accompanied with hydride ion formation, thereby reducing Cs⁺ sites partially or fully, which is inconsistent with the *in situ* Cs L₃-edge XANES spectra unchanged

during the catalysis (Figure 3 (B)). Hence, the association of the superior catalytic property of Cs⁺ single sites to other factors such as the largest size of Cs⁺ ion (0.334 nm) among alkali metal ions and the unaffected Sanderson electro-positivity of Cs⁺ ion is foreordained.^{1,43} This hypothesis is supported by the trend of the ion size effect in the catalytic performance as shown in Figure 2 and by the methyl cyanation experiment of 3-methylpyridine, where neither aldehyde nor cyanide products were produced because perhaps the electro-positivity of Cs⁺ was quenched by lone pair electrons of 3-methylpyridine. The larger electro-positivity and size of Cs⁺ ions stem the lower polarizability or higher softness of Cs⁺ ions are further ensconced by their confinement within zeolite pores.⁴⁴ The polarizability shuffles with the high electro-positivity in the Cs⁺/Y, which, in turn, efficiently copes with the energy penalty to overcome the ammoxidation reaction barriers. There was no change in the Cs⁺ oxidation state during the catalysis, and thus, the mechanism differs from the traditional redox catalysis (eg. Mars-van Krevelen mechanism)⁴⁵ and also acid-base catalysis involving clearly defined interaction modes.

To shed light on the origin of the selective C_{sp3}-H cyanation performance of the Cs⁺ single site/Y catalyst and to understand the ammoxidation mechanism at the molecular level, we performed periodic self-consistent DFT calculations for the reaction pathway. The reaction mechanism, coordination arrangements and energy profiles involving reaction intermediates and transition states for the toluene ammoxidation on Cs⁺ single site in Y zeolite pore are shown in Figure 5 (catalytic cycle outline), Figure S8 (reaction pathway) and Figure S9 (detailed mechanism and energy profiles). The significantly large diameter of Cs⁺ ion enables all three reactant molecules (C₆H₅CH₃, O₂ and NH₃) to get adsorbed on a Cs⁺ single site. It was found that an NH₃ molecule adsorbed/coordinated on a Cs⁺ site promotes the toluene C_{sp3}-H activation and O₂ activation accompanied with the C-O bonding on the Cs⁺ site to produce hydroperoxy intermediate (Int1: C₆H₅CH₂OOH) via transition state TS1, followed by the formation of *gem*-diol intermediate (Int2: C₆H₅CH(OH)₂) gaining a bond rearrangement energy of 233.5 kJ mol⁻¹ (Figure S9). NH₃ plays an important role in the coadsorption of toluene and O₂ on Cs⁺ single site, where donation from NH₃ to Cs⁺ is essential for the interaction between toluene methyl group and O₂ molecule on a Cs⁺ single site. The adsorption behavior and strength of NH₃ was examined by NH₃ TPD (Figure S10). The NH₃ adsorption behavior at the Cs⁺ single sites in zeolite pores cannot be evidenced from the NH₃ TPD curves, but the NH₃ TPD data are compatible with the trend of

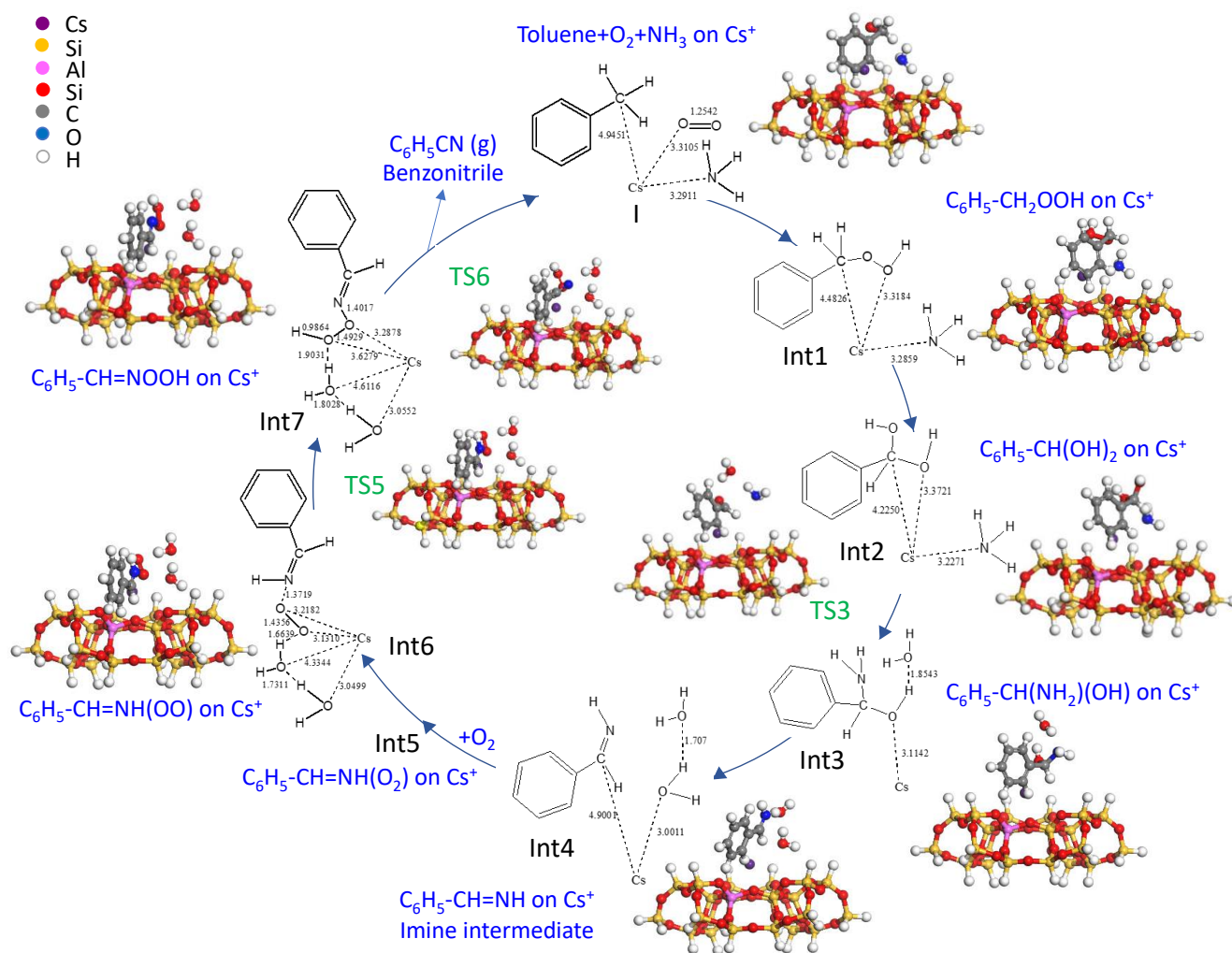


Figure 5. A catalytic cycle (ball-stick model figures) of the ammoxidation of toluene C_{sp}³-H bonds via the inter-coadsorbate reaction pathway without O₂ dissociation and lattice oxygen involvement on a Cs⁺ single site in Y zeolite pore rationalized by DFT calculations involving the reaction intermediates and transition states. Bond distances: see Figure S8 and S9.

Mulliken charges for Cs⁺/Y and Cs⁺/β by DFT and the fact that NH₃ promotes the toluene ammoxidation more with Cs⁺/Y than Cs⁺/β. Then, the Int2 was transformed to aminohydroxytoluene intermediate (Int3: C₆H₅CH(NH₂)(OH)) with C-N bond via a benzaldehyde-type transition state (TS3) that interacts with the coadsorbed NH₃ and H₂O. Hydrogen atom of the C-OH end of Int2 shifts to other O-H group to form TS3 that consists of

distorted benzaldehyde, H₂O and NH₃. In the TS3, benzaldehyde molecule exhibits a nonplanar conformation, where the plane of the phenyl group and the plane of the carbonyl group form an angle of 41.3 degree. It is noted that the stable planar benzaldehyde molecule does not appear in the whole reaction pathways. The Int3 was dehydrated by the inter-ligand bond rearrangement involving N-H bond scission to form imine intermediate (Int4: C₆H₅CH=NH) via C-O breaking transition state (TS4), which is stabilized on the Cs⁺ single site. The imine N atom interacts with the Cs 6s LUMO as electron acceptor,⁴⁶ resulting in the promotion of the reaction with the second adsorbed O₂ at the N position (Int5: C₆H₅CH=NH(O₂) and Int6: C₆H₅CH=NH(OO)) and the inter-ligand rearrangements occur between the two imine H atoms and oxygen successively to produce C₆H₅CH=NOOH intermediate (Int7) via transition state (TS5) and benzonitrile C₆H₅C≡N (F) via transition state (TS6) accompanied with H₂O₂ (readily decomposed to H₂O at 623 K). These inter-ligand bond rearrangements are possible with the large-sized (0.334 nm) Cs⁺ ion. Finally, the adsorbed benzonitrile (F) desorbs to gas phase with a desorption energy 71.0 kJ mol⁻¹ in a gas-phase single-path flow reaction. The rate-determining steps in the whole reaction pathway constitute three C-H and N-H bond dissociation steps (Int1→Int2, Int3→Int4, and Int7→F) after the first dissociation of toluene C_{sp3}-H bonds (Figure S9). In the catalysis mechanism the Cs⁺ single ion sites confined in Y zeolite pores provide a trimolecular assembly platform to enable the coordination-promoted concerted ammoxidation pathway without involvements of O₂-dissociated O atom and lattice oxygen.

4. CONCLUSIONS

Industrial vapor-phase ammoxidation reactions have been extensively studied over mixed transition-metal oxide catalysts with moderate redox potentials and sufficient M–O bond strengths, which bring about active lattice oxygen and oxygen atoms at the catalyst surfaces to promote redox catalysis. However, alkali and alkaline-earth metal ions with noble gas electronic structures have been supposed to be inactive for selective oxidation processes before our recent report on benzene C_{sp2}-H hydroxylation with N₂O or O₂ toward phenol.¹ The Cs⁺ single ion site/Y catalyst without a beneficial redox property, which was inactive for the benzene hydroxylation, showed the unprecedented catalysis with high efficiencies toward catalytic

cyanation (ammoxidation) of C_{sp3}-H bonds of toluene and its derivatives with NH₃ as test reactions. The molar ratios of [NH₃ consumed]/[nitriles synthesized] were nearly stoichiometric, minimizing undesired extra oxidation of NH₃, which is advantageous industrially. DFT calculations indicated the reduction of the HOMO–LUMO gap and the variation of HOMO component by the chemical confinement of Cs⁺ single ion sites in Y zeolite pores making Cs–O(lattice) bonds, which provided a new trimolecular assembly platform to enable the coordination-promoted concerted pathway working closely on the large-sized Cs⁺ single site without any significant change of Cs⁺ charge, different from the traditional redox catalysis mechanisms (e.g. the Mars-van Krevelen mechanism). At the initial stage of the reaction NH₃ plays an important role in the coadsorption of toluene and O₂ on Cs⁺ single sites, where donation from NH₃ to Cs⁺ is essential for the interaction between toluene methyl group and O₂ molecule to form C–O bond on a Cs⁺ single site according to DFT calculations. Then, the neighboring NH₃ molecule joins the ammoxidation reaction, which proceeds successively via several reaction intermediates and transition states with C–N bond, C=N bond and finally C≡N bond on a large-sized Cs⁺ single site confined in Y zeolite pore. Our synthetic strategy potentially increases the scope of on-demand organic nitrile synthesis by rationally incorporating Cs⁺ ions in Y zeolite pores simply by an industrially advantageous facile ion-exchange process.

AUTHOR INFORMATION

Corresponding Author

[*iwasawa@pc.uec.ac.jp](mailto:iwasawa@pc.uec.ac.jp)

Author Contributions

The manuscript was written through contributions of all authors. All authors have given approval to the final version of the manuscript. [‡] These authors contributed equally.

Funding Sources

Grant-in-Aid for Scientific Research of JSPS/MEXT (16F16078 and 16F16383).

Notes

The authors declare no competing financial interests.

ASSOCIATED CONTENT

Tables S1, S2 and S3 for lists of catalytic performance data for Cs⁺/Y with different Si/Al ratios, Cs loadings and catalyst weights, respectively, Figures S1 and S2 for time-on-stream performances (conversion and selectivity) of Cs⁺/Y at 623 K, Figures S3 and S4 for XRD patterns and bright-filed STEM-EDS maps, respectively, Figures S5 and S6 for DFT simulations of optimized structure model of Cs⁺/Y and HOMO-LUMO states, respectively, Figure S7 for TPD curves of CH₃CN and CO₂, Figures S8 and S9 for DFT computational reaction pathways and energy profiles, and Figure S10 for TPD curves of NH₃. This material is available free of charge via the Internet at <http://pubs.acs.org>.

ACKNOWLEDGMENT

The study was supported by Grant-in-Aid for Scientific Research (16F16078 and 16F16383). S. S. A. and S. G. thank JSPS Postdoctoral Fellowship for foreign researchers. The XAFS measurements were performed with the approval of SPring-8 subject number 2017A7808, 2017A7841, 2018A7840, 2018B7840, and 2019A7840.

REFERENCES

1. Ghosh, S.; Acharyya, S. S.; Kaneko, T.; Higashi, K.; Yoshida, Y.; Sasaki, T.; Iwasawa, Y. Confined Single Alkali Metal Ion Platform in a Zeolite Pore for Concerted Benzene C–H Activation to Phenol Catalysis. *ACS Catal.* **2018**, *8*, 11979–11986.
2. Acharyya, S. S.; Ghosh, S.; Yoshida, Y.; Kaneko, T.; Sasaki, T.; Iwasawa, Y. NH₃ -Driven Benzene C-H Activation with O₂ that Opens a New Way for Selective Phenol Synthesis, *Chem. Rec.* **2019**, *19*, 1–14.
3. Cavalli, P.; Cavani, F.; Manenti, I.; Trifiro, F. Ammoxidation of Toluene to Benzonitrile on Vanadium-Titanium Oxides Catalysts Prepared by Precipitation. The Role of Catalyst Composition. *Ind. Eng. Chem. Res.* **1987**, *26*, 639–647.

4. Anbarasan, P.; Schareina, T.; Beller, M. Recent Developments and Perspectives in Palladium-Catalyzed Cyanation of Aryl Halides: Synthesis of Benzonitriles. *Chem. Soc. Rev.* **2011**, *40*, 5049–5067.
5. Sundermeier, M.; Zapf, A.; Mutyala, S.; Baumann, W.; Sans, J.; Weiss, S.; Beller, M. Progress in the Palladium-Catalyzed Cyanation of Aryl Chlorides. *Chem. Eur. A* **2003**, *9*, 1828–1836.
6. Hodgson, H. H. The Sandmeyer Reaction. *Chem. Rev.* **1947**, *40*, 251–277
7. Jagadeesh, R. V.; Junge, H.; Beller, M. Green Synthesis of Nitriles using Non-Noble Metal Oxides-Based Nanocatalysts. *Nat. Commun.* **2014**, *5*, 4123
8. Yang, J.; Karver, M. R.; Li, W.; Sahu, S.; Devaraj, N. K. Metal-Catalyzed One-Pot Synthesis of Tetrazines Directly from Aliphatic Nitriles and Hydrazine. *Angew. Chem.* **2012**, *51*, 5222–5225.
9. Pollak, P.; Romeder, G.; Hagedorn, F.; Gelbke, H. P. Ullman's Encyclopedia of Industrial Chemistry, Wiley-VCH Verlag GmbH & Co. KGaA, Weinheim, 2000, https://doi.org/10.1002/14356007.a17_363
10. Wang, L.; Wang, G.; Zhang, J.; Bian, C.; Meng, X.; Xiao, F. S. Controllable Cyanation of Carbon-Hydrogen Bonds by Zeolite Crystals over Manganese Oxide Catalyst. *Nat. Commun.* **2017**, *8*, 15240.
11. Centi, G.; Marchi, F.; Perathoner, S. Effect of Ammonia Chemisorption on the Surface Reactivity of V-Sb-oxide Catalysts for Propane Ammoxidation. *Appl. Catal. A* **1997**, *149*, 225–244.
12. Otamiri, J. C.; Andersson, A. Kinetics and Mechanisms in the Ammoxidation of Toluene over a V₂O₅ catalyst. Part 1: Selective Reactions. *Catal. Today* **1988**, *3*, 211–222.
13. Rapolu, R.; Panja, K. R. Highly selective V-P-O/ γ -Al₂O₃ Catalysts in the Ammoxidation of Toluene to Benzonitrile. *Chem. Commun.* **1993**, 1175–1176;
14. Sanati, M.; Andersson, A.; Wallenberg, L. R.; Rebenstorf, B. Zirconia-Supported Vanadium Oxide Catalysts for Ammoxidation and Oxidation of Toluene: A Characterization and Activity Study. *Appl. Catal. A* **1993**, *106*, 51–72
15. Martin, A.; Berndt, H. Lücke, B.; Meisel, M. Reaction Pathway of Benzonitrile Formation during Toluene Ammoxidation on Vanadium Phosphate Catalysts. *Top. Catal.* **1996**, *3*, 377–386.

16. Zhang, Y.; Martin, A.; Berndt, H.; Lücke, B.; Meisel, M. FTIR Investigation of Surface Intermediates Formed during the Ammoxidation of Toluene over Vanadyl Pyrophosphate. *J. Mol. Catal. A* **1997**, *118*, 205–214.
17. Martin, A.; Hannour, F.; Brückner, A.; Lücke, B. Ammoxidation of Toluene on Vanadyl Polyphosphates-VO(PO₃)₂, 2. Catalytic Properties. *React. Kinet. Catal. Lett.* **1998**, *63*, 245–251.
18. Younes, M. K.; Ghorbel, A. Catalytic Nitroxidation of Toluene into Benzonitrile on Chromia–Alumina Aerogel Catalyst. *Appl. Catal. A* **2000**, *197*, 269–277.
19. Chary, K. V. R.; Reddy, K. R.; Bhaskar, T.; Sagar, G. V. Dispersion and Reactivity of Mo/Nb₂O₅ Catalysts in the Ammoxidation of Toluene to Benzonitrile. *Green Chem.* **2002**, *4*, 206–209.
20. Rombi, E.; Ferino, I.; Monaci, R.; Picciau, C.; Solinas, V.; Buzzoni, R. Toluene Ammoxidation on α -Fe₂O₃-based Catalysts. *Appl. Catal. A* **2004**, *266*, 73–79.
21. Teimouri, A.; Najari, B.; Chermahini, A. N.; Salavatia, H.; Najafabadi, M. F. Characterization and Catalytic Properties of Molybdenum Oxide Catalysts Supported on ZrO₂– γ -Al₂O₃ for Ammoxidation of Toluene. *RSC Adv.* **2014**, *4*, 37679–37686.
22. Goto, Y.; Shimizu, K.; Kon, K.; Toyao, T.; Murayama, T.; Ueda, W. NH₃-Efficient Ammoxidation of Toluene by Hydrothermally Synthesized Layered Tungsten-Vanadium Complex Metal Oxides. *J. Catal.* **2016**, *344*, 346–353.
23. Bathula, H. B.; Rao, K. T. V.; Suh, Y-W.; Prasad, P. S. S.; Lingaiah, N. One-Step Selective Synthesis of 2-Chlorobenzonitrile from 2-Chlorotoluene via Ammoxidation. *New J. Chem.* **2018**, *42*, 1892-1901.
24. Li, X.; Sun, L.; Hu, M.; Huang, R.; Huang, C. Hydrothermal Synthesis of Urchin-like W-V-O Nanostructures with Excellent Catalytic Performance. *Inorg. Chem.* **2018**, *57*, 14758–14763.
25. Centi, G.; Jiru, P.; Trifiro, F. Catalytic Properties of Zeolites in Oxidation and Ammoxidation Reaction. *Stud Surf Sci Catal.* **1989**, *44*, 247-254
26. Iwasawa, Y.; Asakura, K.; Tada, M. eds., *XAFS Techniques for Catalysts, Nanomaterials and Surfaces*, Springer, Chapter 1 (pp.3-10), Chapter 2 (pp.13-50), Chapter 20 (pp.299-316), **2016**.

27. Ravel, B.; Newville, M. ATHENA, ARTEMIS, HEPHAESTUS: Data Analysis for X-Ray Absorption Spectroscopy using IFEFFIT, *J. Synchrotron Rad.* **2005**, *12*, 537–541.
28. Rehr, J. J.; Albers, R. C. Theoretical Approaches to X-Ray Absorption Fine Structure, *Rev. Mod. Phys.* **2000**, *72*, 621–654.
29. Newville, M.; Ravel, B.; Haskel, D.; Rehr, J. J.; Stern E. A.; Yacoby, Y. Analysis of Multiple-Scattering XAFS Data Using Theoretical Standards. *Physica B Condens* **1995**, 208–209, 154-156.
30. Delly, B. An All-Electron Numerical method for Solving the Local Density Functional for Polyatomic Molecules. *J. Chem. Phys.* **1990**, *92*, 508-517.
31. Delly, B. From Molecules to Solids with the DMol3 Approach. *J. Chem. Phys.* **2000**, *113*, 7756-7764.
32. Perdew, J. P.; Wang, Y. Accurate and Simple Analytic Representation of the Electron-Gas Correlation Energy. *Phys. Rev. B* **1992**, *45*, 13244-13249.
33. Halgren T. A.; Lipscomb, W. N. The Synchronous-Transit Method for Determining Reaction Pathways and Locating Molecular Transition States. *Chem. Phys. Lett.* **1977**, *49*, 225-232.
34. Bell, S.; Crighton, J. S. Locating Transition States. *J. Chem. Phys.* **1984**, *80*, 2464-2475.
35. A-Khattaf, S. Catalytic Transformation of Toluene over a High-Acidity Y-Zeolite Based Catalyst. *Energy Fuels* **2006**, *20*, 946–954.
36. Verboekend, D.; Nuttens, N.; Locus, R.; Van Aelst, J.; Verolme, P.; Groen, J. C.; Pe´rez-Ramirez, J.; Sels, B. F. Synthesis, Characterisation, and Catalytic Evaluation of Hierarchical Faujasite Zeolites: Milestones, Challenges, and Future Directions. *Chem. Soc. Rev.* **2016**, *45*, 3331–3352.
37. Tang, Y.; Li, Y.; Fung, V.; Jiang, D.; Huang, W.; Zhang, S.; Iwasawa, Y.; Sakata, T.; Nguyen, L.; Zhang, X.; Frenkel, A. I.; Tao, F. Single Rhodium Atoms Anchored in Micropores for Efficient Transformation of Methane under Mild Conditions. *Nature Commun.* **2018**, *9*, 1231.
38. Lücke, B.; Narayana, K. V.; Martin, A.; Jähnisch, K. Oxidation and Ammoxidation of Aromatics. *Adv. Synth. Catal.* **2004**, *346*, 1407-1424.
39. Ghosh, S.; Acharyya, S. S.; Tripathi D.; Bal, R. Preparation of Silver–Tungsten Nanostructure Materials for Selective Oxidation of Toluene to Benzaldehyde with Hydrogen Peroxide, *J. Mater. Chem. A* **2014**, *2*, 15726-15733

40. Busca, G.; Cavani, F.; Trifirò, F. Oxidation and Ammoxidation of Toluene over Vanadium-Titanium Oxide Catalysts: A Fourier Transform Infrared and Flow Reactor Study. *J. Catal.* **1987**, *106*, 471-482.
41. Lücke, B.; Martin, A. Catalysis of Organic Reactions, Eds. M.G. Scaros, M. L. Prunier, Marcel Dekker Inc., New York-Basel-Hong Kong, **1994**, p.479-482.
42. Mirth, G.; Cejka, J.; Lercher, J. Transport and Isomerization of Xylenes over HZSM-5 Zeolites. *J. Catal.* **1993**, *139*, 24–33.
43. Keller, T. C.; Desai, K.; Mitchell S.; Pérez-Ramírez, J. Design of Base Zeolite Catalysts by Alkali-Metal Grafting in Alcoholic Media. *ACS Catal.* **2015**, *5*, 5388–5396.
44. Boronat, M.; Corma, A. What Is Measured When Measuring Acidity in Zeolites with Probe Molecules? *ACS Catal.* **2019**, *9*, 1539–1548.
45. Mars, P.; van Krevelen, D. W. Oxidations Carried out by Means of Vanadium Oxide Catalysts. *Chem. Eng. Sci. Suppl.*, **1954**, *3*, 41-59.
46. Zachariasse, K. A.; Grobys, M.; Haar, T.; Der, V.; Hebecker, A.; Ilichev, Y. V.; Morawski, O.; Ruckert, I.; Kuhnle, W. J. Photo-Induced Intramolecular Charge Transfer and Internal Conversion in Molecules with a Small Energy Gap Between S1 and S2. Dynamics and Structure *Photochem. Photobiol. A Chem.* **1997**, *105*, 373-383.

Insert Table of Contents artwork here

